PHYSICAL REVIEW C VOLUME 16, NUMBER 5 NOVEMBER 1977

Elastic electron scattering from the multipole moment distributions of ^{25}Mg†

H. Euteneuer, H. Rothhaas, and O. Schwentker
Institut für Kernphysik, Universität Mainz, 65 Mainz, West Germany

J. R. Moreira
Instituto de Fisica, Universidade de São Paulo, Brazil

C. W. de Jager, L. Lapikás, and H. de Vries
Instituut voor Kernphysisch Onderzoek, Amsterdam, The Netherlands

J. Flanz, K. Itoh, G. A. Peterson, and D. V. Webb
Department of Physics and Astronomy, University of Massachusetts, Amherst, Massachusetts 01003

W. C. Barber and S. Kowalski
Department of Physics, Massachusetts Institute of Technology, Cambridge, Massachusetts 02139
(Received 29 July 1977)

Elastic electron scattering cross sections of ^{25}Mg were measured over a momentum transfer range from 0.19 to 2.56 fm^{-1} at both forward and backward angles. Information on all of the ground state multipole moments of both Coulomb and magnetic character has been obtained.

[NUCLEAR REACTIONS ^{25}Mg(e,e), $E=40.0$–260 MeV, $\theta=28°$–180°; measured $\sigma(E,\theta)$; deduced C0, C2, C4, M1, M3, and M5 moments.]

I. INTRODUCTION

During the past decade, electron scattering has been widely used for the determination of the electromagnetic properties of nuclei. By observing forward- and backward-angle scattering one can learn about both the nuclear charge and current densities. Although a great deal of information has been obtained about nuclear excited states, we shall restrict ourselves here to a discussion of ground state information as determined by elastic electron scattering.

From forward-angle elastic electron scattering the most common ground state parameters extracted pertain to the spherically symmetrical part of the charge distribution, the Coulomb monopole or $C0$ part.[1] From a study of the region of the first $C0$ diffraction minimum some information on the quadrupole or $C2$ part has been obtained for a few light nuclei.[2] At backward angles, magnetic scattering has been observed from magnetic multipole moment distributions up to and including that of the $M9$ moment. The charge scattering provides information about collective properties of nuclei, whereas the magnetic scattering, resulting principally from one or a few nucleons, is a measure of single particle aspects. In preceding experiments information about only some of the moments could be obtained. The improved accuracy of the present work and the appropriate choice of the experimental facilities permitted the extraction of all of the multipole moments of both the charge and magnetic distributions of ^{25}Mg. The charge scattering was measured at forward angles with sufficient accuracy to permit the extraction of the $C0$, $C2$, and $C4$ moments and the magnetic scattering at backward angles so as to obtain information on the magnetic moments $M1$, $M3$, and $M5$.

Three different experimental facilities were used, each of which had particular properties suitable for certain aspects of the measurements. The electron scattering facility of Mainz, Germany, was especially suitable for measuring the forward-angle cross sections with high precision; the 180° scattering apparatus of the Instituut voor Kernphysisch Onderzoek (IKO), Amsterdam, The Netherlands, provided the only means of measuring the $M1$ and $M3$ scattering at low momentum transfers. The higher energy of the Bates accelerator of Middleton, Massachusetts, permitted the measurement of $M3$ and $M5$ scattering at higher momentum transfers.

II. THEORY

In the plane-wave Born approximation (PWBA) the cross section for the elastic scattering of an electron from a nucleus can be simply related to the charge and current densities of the nuclear

ground state. We limit ourselves here to a survey of this simple formalism for illustrative purposes, although in our final data analysis we take into account the distortion of the electron waves by the nuclear Coulomb field.

A. Electron scattering from multipole moment distributions

The PWBA cross section $d\sigma/d\Omega(E,\theta)$ for the scattering of an electron of total energy E through a laboratory angle θ from a nucleus of ground state spin I is given by[3]

$$\frac{d\sigma}{d\Omega}(E,\theta)=\sigma_M(E,\theta)\left[F_L^2+(\tfrac{1}{2}+\tan^2\tfrac{1}{2}\theta)F_T^2\right], \qquad (1)$$

with

$$F_L^2=\sum_{\substack{\lambda=0\\ \text{even}}}^{2I} Q_\lambda^2|F_\lambda^C(q)|^2$$

and

$$F_T^2=\sum_{\substack{\lambda=1\\ \text{odd}}}^{2I} M_\lambda^2\left(\frac{1}{M_p c^2}\right)^2|F_\lambda^M(q)|^2 .$$

Here M_P denotes the proton mass, and $\sigma_M(E,\theta)$ the Mott cross section for an electron to scatter from a point nucleus of mass M_T and of unit charge

$$\sigma_M(E,\theta)=\left(\frac{\alpha\hbar c}{2E}\right)^2\frac{\cos^2\tfrac{1}{2}\theta}{\sin^4\tfrac{1}{2}\theta}\eta ,$$

where the recoil factor $\eta=[1+(2E/M_Tc^2)\sin^2\tfrac{1}{2}\theta]^{-1}$. The Coulomb form factor $F_\lambda^C(q)$ with the corresponding Coulomb multipole moment Q_λ of order λ, and the magnetic form factor $F_\lambda^M(q)$ with the corresponding magnetic multipole moment M_λ, contain all of the information about the nuclear charge and current densities. These form factors are functions of the momentum transferred to the nucleus by the electron, $q=(2E/\hbar c)\sqrt{\eta}\sin\tfrac{1}{2}\theta$. The multipole moments are restricted by conservation of angular momentum to $\lambda\leq 2I$. Parity conservation and time-reversal invariance further require that only even Coulomb multipoles, $C0$, $C2,\ldots$, and odd magnetic multipoles, $M1$, $M3,\ldots$, contribute to the scattering. We will use the convention

$$Q_\lambda=\left(\frac{4\pi}{2\lambda+1}\right)^{1/2}\int r^\lambda\rho(\vec{r})Y_\lambda^0(\hat{r})d^3r$$

and

$$M_\lambda=\left(\frac{4\pi\lambda}{(2\lambda+1)(\lambda+1)}\right)^{1/2}\int r^\lambda\vec{j}(\vec{r})\cdot\vec{Y}_{\lambda,\lambda}^{0}(\hat{r})d^3r$$

so as to obtain $Q_0=Z$, the nuclear charge, $Q_2=\tfrac{1}{2}Q$, where Q is the quadrupole moment, and $M_1=\mu$, the magnetic dipole moment. The charge and current densities are given in terms of the multipole densities:

$$\rho(\vec{r})=\sum_{\substack{\lambda=0\\ \text{even}}}^{2I}\begin{pmatrix} I & \lambda & I\\ I & 0 & -I\end{pmatrix}\rho_\lambda(r)Y_\lambda^{0*}(\hat{r})$$

and

$$\vec{j}(\vec{r})=\sum_{\substack{\lambda=1\\ \text{odd}}}^{2I}\sum_{\lambda'}\begin{pmatrix} I & \lambda & I\\ I & 0 & -I\end{pmatrix}j_{\lambda,\lambda'}(r)\vec{Y}_{\lambda,\lambda'}^{0*}(\hat{r}).$$

The Coulomb and magnetic contributions to the cross section given in Eq. (1) may be separated experimentally because of their different dependence on θ. However, all of the individual multipole form factors of these two contributions add incoherently if the electron beam is not polarized and the polarization of the recoil nucleus is not observed. Therefore it is impossible in this type of experiment to separate the individual multipole contributions in a model-independent way. Nevertheless, calculations using various nuclear models indicate that the form factors of different multipoles dominate at different q; generally, the higher the multipole, the higher the q where its form factor dominates. In the next sections different models used for the determination of the multipole distributions are discussed.

B. Multipole moment distributions

Since all of the charged particles in the nucleus contribute to the Coulomb multipole moments, we have used a phenomenological collective model for the charge distribution as was suggested by Überall,[4] where

$$\rho_\lambda(r)=\begin{cases}[4\pi(2I+1)]^{1/2}\rho(r), & \lambda=0,\\ N_\lambda\begin{pmatrix} I & \lambda & I\\ I & 0 & -I\end{pmatrix}^{-1}r^{\lambda-1}\dfrac{d}{dr}\rho(r), & \lambda\neq 0,\end{cases}$$

where the N_λ are normalization parameters which are related to the deformation of the nucleus. For $\rho(r)$ we used the phenomenological three-parameter Fermi distribution

$$\rho(r)=\frac{1+w(r/c)^2}{1+\exp[(r-c)/z]}.$$

Since the magnetic moments of the nuclear ground state are generated mainly by the valence nucleons, we have used a shell model (SM) for their calculation. The nuclear current density is a sum of a convection current part and an intrinsic spin magnetization part:

$$\vec{j}_\lambda(\vec{r})=\vec{j}_\lambda^{c}(\vec{r})+\vec{\nabla}\times\vec{\mu}_\lambda^{s}(\vec{r}).$$

Consequently the magnetic form factor contains an orbital or g_l component and an intrinsic magnetization or g_s component[3]:

$$F_\lambda^M(q) \propto [g_l A_\lambda \langle nl | j_{\lambda-1}(qr) + j_{\lambda+1}(qr) | nl \rangle$$
$$\mp \tfrac{1}{2} g_s \langle nl | j_{\lambda-1}(qr) - B_\lambda j_{\lambda+1}(qr) | nl \rangle)]$$
$$\times F(q)_{\text{nucl}} F(q)_{\text{c.m.}} ,$$

for $l = j \pm 1/2$. The matrix elements $\langle nl | j_\lambda(qr) | nl \rangle \equiv \int R_{nl}^2 j_\lambda(qr) r^2 dr$ contain the spherical Bessel functions $j_\lambda(qr)$ of order λ and the radial shell-model wave functions $R_{nl}(r)$ of the nucleon. The form factors $F(q)_{\text{nucl}}$ and $F(q)_{\text{c.m.}}$ account for the finite size of the nucleon and for the motion of the center of mass of the nucleus, respectively. The constants A_λ and B_λ are given by

$$A_\lambda = \frac{2l+1 \pm \lambda}{\lambda+1}$$

and

$$B_\lambda = \frac{\lambda}{\lambda+1} \frac{2l+1 \pm \lambda}{2l+1 \mp (\lambda+1)} \qquad \text{for } l = j \pm \tfrac{1}{2}.$$

For a free nucleon the gyromagnetic ratios are $g_l = 1$ and 0 and $g_s = 5.59$ and -3.83 for a proton and a neutron, respectively.

In the extreme single particle model (ESPM), the magnetic moment of ^{25}Mg is completely generated by a $1d_{5/2}$ neutron, and consequently the orbital convection current part vanishes. However, the experimental static dipole moment ($\mu = 0.855\mu_N$)[5] deviates strongly from the Schmidt value ($-1.91\mu_N$). Although this can be accounted for by introducing a pure quenching of the g_s factor of the neutron, it is more realistic to use a more complete shell-model calculation where the magnetic moment is generated by all valence nucleons. In the simplest approach one can assume that the magnetic moment is generated by all of the particles in the $1d_{5/2}$ shell, protons as well as neutrons. By only allowing states with seniority one, we can describe the ground state for ^{25}Mg using the extreme single particle model with effective gyromagnetic ratios $g_l = +0.19$ and $g_s = -2.04$.[6] This so-called individual particle model (IPM) yields a dipole moment of $-0.64\mu_N$.

Recent shell-model calculations[7] which allowed the valence particles to occupy the full $2s_{1/2}$, $1d_{3/2}$, and $1d_{5/2}$ shells predict a dipole moment of $-0.74\mu_N$ if the Kuo two-body interaction is used, and $-0.79\mu_N$ for the Preedom and Wildenthal interaction. We have compared our experimental results with the Michigan State University shell-model calculations performed with the Oak Ridge-Rochester computer code. In these calculations a semi-empirical model has been used for the determination of the one- and two-body matrix elements.[8] According to this calculation the magnetic dipole moment is $-0.85\mu_N$.

The differences between these models are apparent from Fig. 1, where the total current distribution $j_\lambda(r)$, the sum of the intrinsic and the orbital currents, is given. This figure shows that all magnetic moments resulting from both the IPM and the SM calculations are strongly quenched with respect to the extreme single particle, $1d_{5/2}$ neutron model. In Table I we have given the predictions for the static magnetic moments for all three models. Throughout these calculations a value of 1.831 fm has been used for the harmonic-oscillator parameter b.

III. EXPERIMENTAL PROCEDURES

The measurements were performed at three different experimental facilities in order to obtain the optimum accuracy for the determination of the parameters of the multipole distributions.

(i) The 300 MeV electron scattering facility at Mainz[9] was used for the study of the Coulomb scattering ($C0$, $C2$, $C4$). In this part of the experiment primary energies between 77 and 250 MeV and scattering angles between 28° and 110° were used.

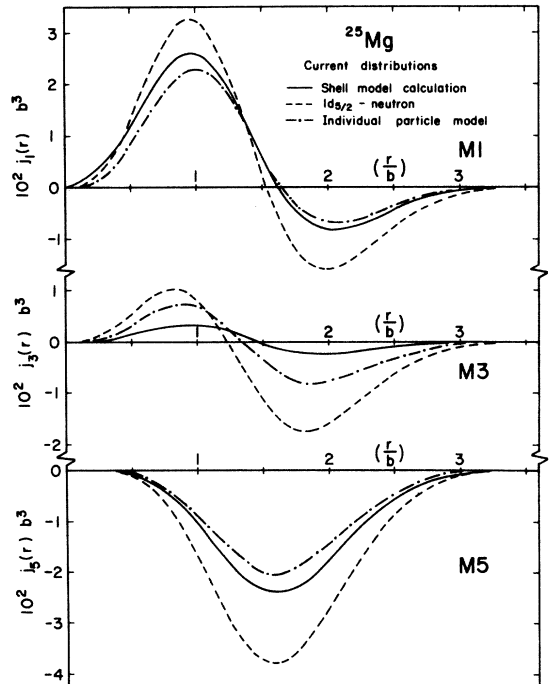

FIG. 1. Current distributions of the magnetic multipole moments for different models. The dashed curves represent the extreme single particle model; the dashed-dotted curves the individual particle model, where the moments are generated by four protons and five neutrons in the $1d_{5/2}$ shell; and the solid curves the shell model calculations of Ref. 8, where all nine valence particles can occupy the complete $2s$-$1d$ shell.

The total resolution was 0.1% full width at half-maximum (FWHM), thus permitting a clear separation of the elastic peak from the peak due to the excitation of the lowest excited state at 590 keV. Beam currents between 10 nA and 20 μA were used. The scattering from a ^{12}C target of 81.79 mg/cm^2 was measured under the same experimental conditions for normalization purposes. A split-foil secondary emission monitor[10] was used for stabilizing the beam position at the target. The effective target thickness was constantly monitored by measuring the scattering at a forward angle of 28° with a fixed-angle spectrometer.[11]

(ii) The 180° scattering apparatus[12] which is part of the 100 MeV electron scattering facility[13] at the IKO in Amsterdam was used for the study of the scattering from the magnetic dipole and octupole moments. Primary electron energies between 40 and 90 MeV were used. The beam current was between 10 and 20 μA. A total resolution of 0.35% assured a clean separation of elastic from inelastic scattering. The magnetic cross sections are extremely small compared to the charge cross sections, even at 180°. In order to determine the charge contribution to scattering from ^{25}Mg accurately, the scattering from a 63.79 mg/cm^2 natural Mg target was also observed.

(iii) Finally, the cross sections for magnetic scattering were determined at q values between 1.20 and 2.56 fm^{-1} with the electron scattering facility[14] of the Bates linear accelerator.[15] The measurements were performed at energies between 120 and 260 MeV. A polyethylene target of 25.09 mg/cm^2 was used as a reference target. The cross sections were measured at a far backward (160°) angular setting of the spectrometer.

The same ^{25}Mg target, isotopically enriched to 99.2%, was used throughout the experiment. Its average thickness was 63.07 mg/cm^2. The homogeneity was accurately determined with an x-ray absorption technique.[16] The differences in thickness over the whole target area turned out to be ± 5%, but in the region of the beam spot the thickness could be well established with an error of 0.5%.

TABLE I. The static magnetic multipole moments predicted by three model calculations: the extreme single particle model (ESPM), the independent particle model (IPM), and the shell model (SM) calculation of Ref. 8.

	ESPM	IPM	SM
Magnetic dipole moment μ (μ_N)	−1.91	−0.63	−0.85
Magnetic octupole moment Ω (μ_N fm^2)	−19.19	−9.21	−2.69
Magnetic triakontaduopole moment Γ (μ_N fm^4)	−56.2	−29.8	−35.4

IV. ANALYSIS

The theoretical formulas given in Sec. II have been derived by using the plane-wave Born approximation (PWBA). For a quantitative analysis of the data this formalism is inadequate because it does not account for the distortion of the electron wave functions by the Coulomb field of the nucleus. We have taken these effects into account by performing an exact calculation of the monopole scattering in a phase shift analysis,[17] whereas for the higher order multipole moments the distorted-wave Born approximation (DWBA) has been used.[18] The cross sections were determined from the area under the elastic peaks after applying radiative corrections.[19] Since the procedures used in the analysis of the charge and the magnetic parts are different, we will describe these procedures separately.

A. Charge scattering

For the forward-angle data ^{12}C was used as a reference nuclide.[20] The cross sections for ^{25}Mg are presented in Table II. Before extracting the charge multipole parameters from these data, the small magnetic scattering contributions, as derived from a fit to the backward-angle high-q data, were subtracted from the highest-q data. These contributions never exceeded 8%.

A first approximation of the parameters for the monopole distribution was determined by analyzing only the cross sections at low q values ($q \leq 1.0$ fm^{-1}). The quadrupole contribution ($C2$) in this region was calculated in DWBA according to the phenomenological quadrupole distribution $\rho_2(r)$ of Sec. II. Here we used a value of $Q = 22\ e\ \text{fm}^2$ for the static quadrupole moments as measured in an atomic beam experiment,[21] and the Fermi distribution parameters of ^{24}Mg [$c = 3.1421(47)$ fm, $z = 0.6047(61)$ fm, $w = -0.1926(42)$][22] which were determined from the simultaneously measured ^{24}Mg cross sections. This procedure is justified because of the small $C2$ contributions (<5%) in this q region. After subtracting the $C2$ contributions from the low-q data, the monopole charge ($C0$) parameters were determined from a fit to the remainder.

Next the $C0$ contribution corresponding to these parameters was calculated for all data and subsequently subtracted. The remainder was then attributed to the $C2$ and $C4$ components, and was

TABLE II. Cross sections determined in the charge scattering experiment. The last column gives the statistical error. The data are corrected for finite spectrometer aperture.

E (MeV)	θ (deg)	$d\sigma/d\Omega$ (fm^2/sr)	$\Delta d\sigma/d\Omega$ (%)	E (MeV)	θ (deg)	$d\sigma/d\Omega$ (fm^2/sr)	$\Delta d\sigma/d\Omega$ (%)
76.93	28	0.3236×10	0.60				
				249.80	40	0.6213×10^{-2}	1.00
90.73	28	0.2224×10	0.60		42.5	0.3538×10^{-2}	0.90
					45	0.1885×10^{-2}	1.00
100.03	28	0.1769×10	0.60		47.5	0.1054×10^{-2}	1.00
	40	0.3481	0.54		50	0.5507×10^{-3}	1.00
	45	0.1957	0.60		52.5	0.2741×10^{-3}	1.00
	50	0.1123	0.80		55	0.1363×10^{-3}	1.10
	55	0.6751×10^{-1}	0.90		57.5	0.6782×10^{-4}	1.00
	60	0.4130×10^{-1}	0.80		60	0.3358×10^{-4}	1.00
	65	0.2554×10^{-1}	0.90		62.5	0.1812×10^{-4}	1.10
	70	0.1604×10^{-1}	0.80		65	0.1093×10^{-4}	1.20
	75	0.1005×10^{-1}	0.90		67.5	0.7629×10^{-5}	1.20
	80	0.6569×10^{-2}	0.80		70	0.6167×10^{-5}	1.10
	90	0.2738×10^{-2}	0.60		72.5	0.5506×10^{-5}	1.20
	100	0.1159×10^{-2}	0.80		75	0.4745×10^{-5}	1.10
	110	0.5044×10^{-3}	0.80		77.5	0.4151×10^{-5}	1.00
					80	0.3514×10^{-5}	1.20
119.23	28	0.1142×10	0.60		82.5	0.2867×10^{-5}	1.40
					85	0.2347×10^{-5}	1.70
139.95	28	0.7481	0.60		87.5	0.1861×10^{-5}	1.90
	45	0.6268×10^{-1}	1.10		90	0.1453×10^{-5}	2.00
	50	0.3241×10^{-1}	1.20		92.5	0.1118×10^{-5}	2.10
	55	0.1652×10^{-1}	1.30		95	0.8943×10^{-5}	2.30
	60	$0.877^{\prime}\ 10^{-2}$	1.00		97.5	0.6466×10^{-5}	2.40
	65	$0.469\text{5}\ 10^{-2}$	0.90		100	0.4853×10^{-5}	3.30
	70	0.2591×10^{-2}	1.00		102.5	0.3599×10^{-5}	2.60
	75	0.1383×10^{-2}	1.00		105	0.2666×10^{-5}	2.60
	80	0.7326×10^{-3}	1.00		110	0.1456×10^{-5}	4.10
	90	0.2128×10^{-3}	1.00				
	100	0.5644×10^{-4}	1.00				
	110	0.1553×10^{-4}	0.90				

fitted with $Q2$ and $Q4$ as free parameters while using the previously determined $C0$ parameters. The multipole contributions were basically calculated in PWBA, but a Coulomb correction factor $C_C = \sigma^{\mathrm{DWBA}}(E,\theta)/\sigma^{\mathrm{BA}}(E,\theta)$ has been applied.[23] From the fitted parameters the DWBA predictions were calculated. The resulting $C2$ and $C4$ contributions were then subtracted from all data points, and the remainder was used as a starting point for a second iterative step. The results of this analysis are presented in Table III. The errors result from trying many different sets of Fermi distribution parameters which, after performing the above iterative procedure, give an acceptable description ($\chi^2/p \leq 2$) of the data over the complete q range. In addition, we have included in Table III existing results for the $C0$ distribution from electron scattering[24] and muonic x rays.[25]

B. Magnetic scattering

In the 180° experiments the cross sections were measured using the established values of the solid angle, detector efficiencies, etc.[12] In the 160° experiments the cross sections were determined relative to those of the proton.[26]

For the analysis of the magnetic multipole cross sections, both data sets had to be corrected for the charge contribution. The charge scattering at 180° was determined from the measured pure charge scattering from ^{24}Mg. An extensive description of this subtraction procedure is given elsewhere.[27] The charge contribution ranged between 99% at 40 MeV to 80% at 90 MeV. For the 160° data points the expected charge cross section was calculated according to the charge parameters determined from the forward-angle experiment. Essentially, this amounted to a transformation of the measured forward-angle cross sections to equivalent q values at backward angles. This procedure was rather insensitive to the relative errors in the various charge multipoles because of the large correlations in their errors. The charge contribution varied from about 84% at 140 MeV to about 12% at 260 MeV.

TABLE III. Charge distribution parameters.

Monopole (CO) distribution				
$\langle r^2\rangle^{1/2}$ (fm)	c (fm)	z (fm)	w	
3.003 ± 0.011	3.218 ± 0.052	0.585 ± 0.043	-0.236 ± 0.034	(e,e) (This work)
3.11 ± 0.05	2.76 ± 0.05	0.608 ± 0.032		(e,e) (Ref. 24)
3.01 ± 0.03				Muonic x rays (Ref. 25) nat_{Mg}

Quadrupole moment:

$|Q| = 2|Q2| = 24.4^{+0.8}_{-4.0}\ e\,\mathrm{fm}^2$ (this work)

$= 22\ e\,\mathrm{fm}^2$ (Ref. 22).

Hexadecapole moment:

$|Q4| = 15.3^{+2.3}_{-10.0}\ e\,\mathrm{fm}^4$.

The magnetic form factors F_T^2 obtained from the 180° experiment are given in Table IV. The columns labeled "stat" and "syst" give the statistical and systematic errors, respectively. The systematic errors include uncertainties in the subtraction of the Coulomb cross section, and in the normalization (target thickness, solid angle, etc.). In Table V the total form factor $F_{\mathrm{tot}}^2 = F_L^2 + (\frac{1}{2} + \tan^2\frac{1}{2}\theta)\, F_T^2$ is given for the 160° experiment together with the deduced magnetic form factors. The errors quoted are the linear sum of the statistical errors (3–13%), the systematic errors due to uncertainties in the proton cross section (4%), and the uncertainties in the subtraction of the Coulomb form factors (10%).

The magnetic form factors obtained were analyzed in PWBA after transforming the experimental q values to effective momentum transfer values by using

$$q_{\mathrm{eff}} = q(1 + f_c Z\alpha\hbar c/ER), \qquad (2)$$

where R is the equivalent radius related to the rms radius of the charge distribution by $R^2 = \frac{5}{3}\langle r^2\rangle$. Here we have determined f_c empirically by comparing DWBA and PWBA calculations; for ^{25}Mg it turned out that with $f_c = 1.20$, an excellent overlap between DWBA and PWBA form factors was obtained for all magnetic multipoles for the range of momentum transfers of this experiment. In the analysis both harmonic oscillator (HO) and Woods-Saxon (WS) wave functions were used.

TABLE IV. Transverse form factors (180°).

E (MeV)	q_{eff} (fm^{-1})	F_T^2 ($\times 10^{-4}$)	Stat (%)	Syst (%)
40	0.459	5.97	62	79
55	0.610	4.42	48	37
60	0.661	3.30	57	36
65	0.711	2.22	32	39
70	0.761	2.40	66	26
75	0.812	4.15	32	10
80	0.862	4.66	37	7
85	0.912	2.68	56	8
90	0.963	3.92	43	4

V. DISCUSSION

The charge parameters given in the preceding section have been obtained for a three-parameter Fermi distribution. The fit to the data is shown in Fig. 2. The monopole data were also analyzed in terms of a Fourier-Bessel expansion.[28] The resulting charge distribution of this "model-independent" analysis is given in Fig. 3, together with the $C2$ and $C4$ distributions as determined by the derivative of the Fermi distribution given in Table III. Within error these results agree with those obtained by taking the derivative of each Fourier-Bessel distribution fitting the data.

We have also analyzed the data with an extreme single particle model using a harmonic oscillator $1d$ wave function and effective charges. This model, however, cannot simultaneously describe the measured electron cross sections and the known quadrupole moment.

TABLE V. Transverse form factors (160°).

E (MeV)	q_{eff} (fm^{-1})	F_{tot}^2	F_T^2 ($\times 10^{-3}$)	ΔF_T^2 (%)
140	1.442	1.60×10^{-1}	7.75×10^{-1}	15
160 (I)	1.639	1.77×10^{-1}	1.03	15
160 (II)	1.639	1.76×10^{-1}	9.82×10^{-1}	15
170	1.738	1.67×10^{-1}	1.44	15
180	1.836	1.40×10^{-1}	1.70	15
200	2.033	6.97×10^{-2}	1.27	15
220	2.229	3.71×10^{-2}	9.20×10^{-1}	+12, −30
240	2.425	1.37×10^{-2}	3.82×10^{-1}	+13, −16
260	2.621	1.24×10^{-2}	3.35×10^{-1}	+18, −10

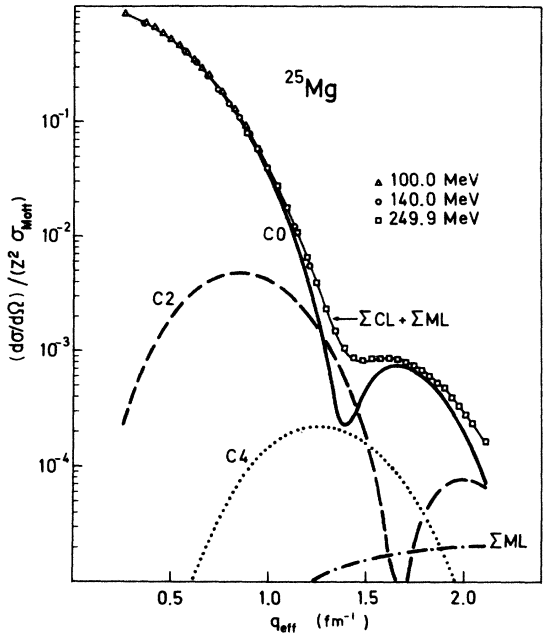

FIG. 2. Ratio between the measured cross sections for charge scattering and Z^2 times the Mott cross section versus q_{eff}, the effective momentum transfer. The solid curve represents the best fit to the data for a Fermi distribution. The individual charge multipoles are also indicated. The curve labeled $\sum ML$ represents the magnetic scattering at 250 MeV as-calculated from backward angle data.

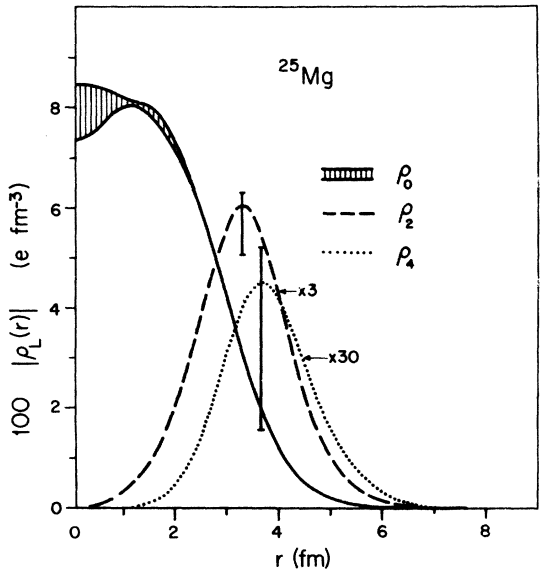

FIG. 3. Multipole density distributions for the individual charge multipoles. The shaded area represents the C0 distribution with its error band as determined from the Fourier-Bessel analysis. The dashed and the dotted curves show the quadrupole and hexadecapole moment distribution, respectively. The shape of these distributions has been taken to be the derivative of a Fermi distribution as explained in the text. The error bars indicate the uncertainties in the distributions.

The results for the complete multipole charge distributions are model dependent, and the errors of the quadrupole and hexadecapole moments given in this paper refer only to uncertainties which follow from systematic examinations within the model described above. However, the good agreement of the value of the determined quadrupole moment with that of the atomic beam experiment[21] gives confidence in the quadrupole density. Due to the high precision with which the charge scattering cross section has been measured over a wide range of momentum transfer, we have been able to extract for the first time ground state parameters for the hexadecapole distribution, together with the quadrupole and monopole distributions.

From the current distributions described in Sec. II, the magnetic form factor $F_T^2(q)$ was calculated for all three models used (ESPM, IPM, and SM) with harmonic oscillator radial wave functions. In Fig. 4 these results are compared with the experimental data. Although both the IPM and the SM calculations yield a strong improvement over the ESPM predictions, the agreement with the data is hardly satisfactory. The q dependence of especially the $M5$ moment differs markedly

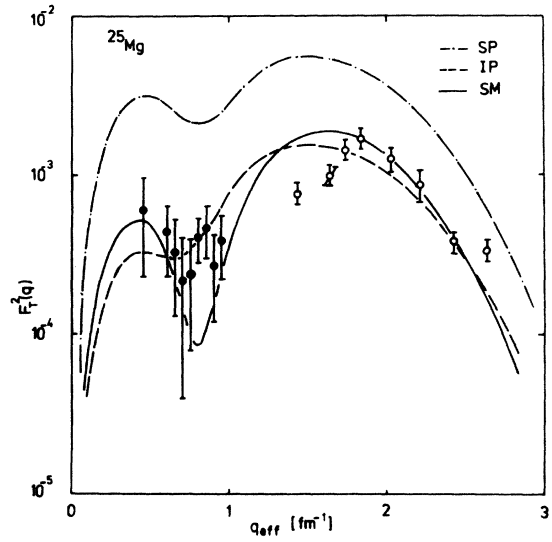

FIG. 4. Comparison between the present experimental data and theoretical predictions for the magnetic form factor. The dashed-dotted curve indicates the extreme single particle model prediction, the dashed curve that of the individual particle model, and the solid curve that of the shell model calculation of Ref. 8. The solid circles denote data taken at 180° and the open circles data taken at 160°.

TABLE VI. Results of the analysis in the generalized single particle model, where α_λ denotes the quenching factor of the magnetic multipole moments with respect to the extreme single particle model prediction. All numbers include systematic errors. The symbols HO and WS refer to the use of harmonic oscillator and Woods-Saxon radial wave functions, respectively. $M_3 = 3.9 \pm 2.6\ \mu_N \mathrm{fm}^2$, $M_5 = 28 \pm 11\ \mu_N \mathrm{fm}^4$, including model dependence (WS − HO).

Model	α_1	α_3	α_5	$\langle r^2 \rangle_{1d}^{1/2}$ (fm)	$\chi^2/(N-P)$
9SPM/HO	0.455	0.22 ± 0.13	0.47 ± 0.03	2.98 ± 0.07	25.1/15
9SPM/WS	0.455	0.27 ± 0.12	0.50 ± 0.08	3.18 ± 0.08	23.8/15

from the experimentally observed behavior.

The data were finally analyzed with a generalized version of the single particle model (GSPM), where the q dependence is still given by a $1d_{5/2}$ radial wave function for a single neutron, but the static multipole moments, except for the dipole moment, were used as free normalization parameters. The magnetic dipole moment was fixed to its experimental value ($-0.855\mu_N$). Both harmonic oscillator (HO) and the Woods-Saxon (WS) wave functions were used for the radial behavior of the valence particle. This leaves three parameters to be determined from the fit: the size parameter b or r_0 for the HO or WS wave functions, respectively, and $M3$ and the $M5$ moments. The skin thickness a_0 of the WS well and the $1d$-shell separation energy E_{sep} were fixed at 0.65 fm and −7.332 MeV (the experimentally determined value for a neutron), respectively.

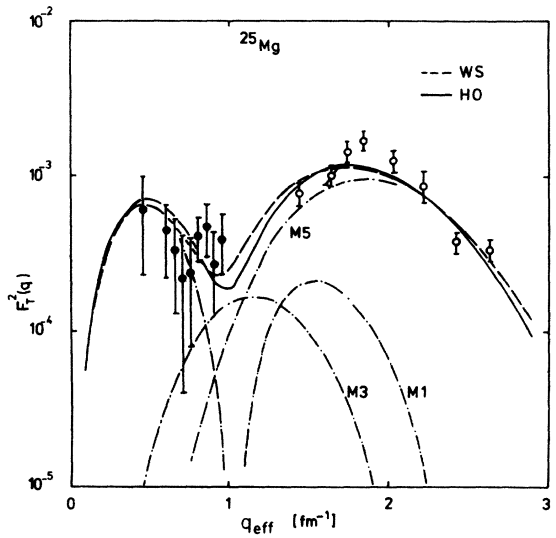

FIG. 5. The magnetic form factor data taken at 180° (solid circles) and at 160° (open circles). The solid curve represents the best fit for the generalized single-particle model with harmonic oscillator wave functions, and the dashed curve that with Woods-Saxon wave functions. The dashed-dotted curves indicate the individual multipole moment contributions with Woods-Saxon radial wave functions.

The sensitivity to a_0 and E_{sep} was estimated by performing separate fits with values of 0.50 fm for a_0 and −14 MeV for E_{sep}. The quality of the fit did not change, while the resulting values of the $M3$ and $M5$ moments and r_0 were consistent with those of the original fit. The results of the final fit are presented in Table VI and in Fig. 5. The quality of the fit is quite good ($\chi^2/(N-P) = 1.6$). No preference is found for either HO or WS wave functions. For a more accurate determination of the $M3$ moment, additional data are needed in the q range between 0.9 and 1.8 fm^{-1}. These can, however, only be obtained from 180 scattering experiments. At present no facility is available for such an experiment.

The good agreement between the quenching factor obtained in the IPM, SM, and GSPM indicate that the $M5$ moment can be described quite well by a single $d_{5/2}$ neutron; therefore, an interesting comparison can be made with magnetic scattering from the $M5$ moment in ^{27}Al which is generated mainly by a $1d_{5/2}$ proton. A comparison with the existing data[27] seems to indicate a somewhat larger radial size for the neutron orbit. More extensive and accurate data, especially for ^{27}Al, are needed in order to investigate the difference between the proton and neutron radii more carefully.

We thank W. Chung and B. H. Wildenthal (Michigan State University) for providing the results of their shell-model calculations prior to publication, and L. E. Wright (Ohio University) for the use of his DWBA computer program.

†Work supported in part by the Deutsche Forschungsgemeinschaft, the Brazilian Conselo Nacional de Desenvolvimento Cientifico e Tecnologico, the Dutch Foundation for Fundamental Research on Matter (FOM), the Netherlands Organization for the Advancement of Pure Research (ZWO), the United States Energy Research and Development Administration, and the U.S. National Science Foundation.

[1]C. W. de Jager, H. de Vries, and C. de Vries, At. Data Nucl. Data Tables 14, 479 (1974).
[2]U. Meyer-Berkhout, K. W. Ford, and A. E. S. Green, Ann. Phys. (N.Y.) 8, 119 (1959).
[3]T. deForest, Jr., and J. D. Walecka, Adv. Phys. 15, 1 (1966).
[4]H. Überall and P. Ugincius, Phys. Rev. 178, 1565 (1969).
[5]F. Alder and F. C. Yu, Phys. Rev. 82, 105 (1951).
[6]A. de-Shalit and I. Talmi, *Nuclear Shell Theory* (Academic, New York and London, 1963); p. 449.
[7]B. J. Cole, A. Watt, and R. R. Whitehead, J. Phys. G1, 17 (1975).
[8]W. Chung, Ph.D. thesis, Michigan State University, 1976 (unpublished).
[9]H. Ehrenberg *et al.*, Nucl. Instrum. Methods 105, 253 (1972).
[10]D. Richter, Diplomarbeit, Universität Mainz, 1970 (unpublished).
[11]H. M. Stolz, Diplomarbeit, Universität, Mainz, 1973 (unpublished).
[12]G. J. C. van Niftrik, H. de Vries, L. Lapikas, and C. de Vries, Nucl. Instrum. Methods 93, 301 (1971).
[13]C. de Vries and P. J. T. Bruinsma, Nucl. Instrum. Methods 74, 5 (1969), and following papers.
[14]S. Kowalski *et al.*, 1967 Summer Study, Medium Energy Nuclear Physics with Electron Accelerators, Report No. TID-24667, USAEC, 1967 (unpublished).
[15]J. Haimson, IEEE Trans. Nucl. Sci. 20, 914 (1973).
[16]K. Chmillon, Diplomarbeit, Universität Mainz 1973 (unpublished).
[17]B. Dreher (private communications).
[18]J. F. Prewitt and L. E. Wright, Phys. Rev. C 9, 2033 (1974).
[19]L. C. Maximon, Rev. Mod. Phys. 41, 193 (1969).
[20]K. Merle, Ph.D. thesis, Universität Mainz, 1976 (unpublished).
[21]A. Lurio, Phys. Rev. 126, 1768 (1962).
[22]H. Euteneuer, G. A. Peterson, H. Rothhaas, and O. Schwentker (unpublished).
[23]O. Schwentker, Ph.D. thesis, Universität Mainz, 1977 (unpublished).
[24]E. W. Lees, C. S. Curran, S. W. Brain, W. A. Gillespie, A. Johnston, and R. P. Singhal, J. Phys. G2, 105 (1976).
[25]G. Backenstoss, S. Claralambus, H. Daniel, H. Coch, G. Polexz, H. Schmitt, and L. Tauscher, Phys. Lett. 25B, 547 (1967).
[26]T. Janssens, R. Hofstadter, E. B. Hughes, and M. R. Yearian, Phys. Rev. 142, 922 (1965).
[27]L. Lapikás, A. E. L. Dieperink, and G. Box, Nucl. Phys. A203, 609 (1973).
[28]B. Dreher, J. Friedrich, K. Merle, H. Rothhaas, and G. Lührs, Nucl. Phys. A235, 219 (1974).